The Lidars in Flat Terrain (LIFT) Experiment

Stephen A. Cohn,* Shane D. Mayor,*,@ Christian J. Grund,+,&
Tammy M. Weckwerth,* and Christoph Senff#

ABSTRACT

The authors describe and present early results from the July–August 1996 Lidars in Flat Terrain (LIFT) experiment. LIFT was a boundary layer experiment that made use of recently developed Doppler, aerosol backscatter, and ozone lidars, along with radars and surface instrumentation, to study the structure and evolution of the convective boundary layer over the very flat terrain of central Illinois. Scientific goals include measurement of fluxes of heat, moisture, and momentum; vertical velocity statistics; study of entrainment and boundary layer height; and observation of organized coherent structures. The data collected will also be used to evaluate the performance of these new lidars and compare measurements of velocity and boundary layer height to those obtained from nearby radar wind profilers. LIFT was a companion to the Flatland96 experiment, described by Angevine et al.

1. Introduction

The atmospheric boundary layer (ABL) is "that part of the troposphere that is directly influenced by the presence of the earth's surface, and responds to surface forcings with a timescale of about an hour or less" (Stull 1988). Mixing in the ABL can be driven by surface heating (free convection) and wind shear (forced convection). A capping inversion usually limits the depth of the daytime convective boundary layer (CBL) to approximately 1–3 km. The ABL connects the earth's surface with the overlying atmosphere. Turbulent motions within it control fluxes of heat, moisture, trace gases, pollution, and momentum. Study of the ABL is important for reasons ranging from improving short-range weather forecasts to understanding global climate change. Also, we spend our lives in this part of the atmosphere.

The first observations of the ABL were obtained primarily using towers, balloons, and kites (e.g., Lewis 1997). Instrumented aircraft and radar wind profilers have been used to reach higher, providing in situ and remotely sensed observations throughout the entire boundary layer. Examples of boundary layer measurements and instrumentation may be found in Kaimal et al. (1976), Lenschow (1970), Young (1988), and Angevine et al. (1994). These various measurement systems have different advantages and limitations and when used together are complementary. The Lidars in Flat Terrain (LIFT) experiment used three modern lidars and two types of radars to study the CBL and its morning and evening transitions.

LIFT was a companion experiment to the Flatland96 experiment described by Angevine et al. (1998). Flatland96 used three 915-MHz wind profilers, one rawinsonde system, and three enhanced surface flux measurement stations (Flux-PAM) and focused on the study of the boundary layer top and entrainment zone. Flatland96 and LIFT took place close to the Flatland Atmospheric Observatory near Urbana,

*National Center for Atmospheric Research, Boulder, Colorado.
+National Oceanic and Atmospheric Administration, Boulder, Colorado.
#Cooperative Institute for Research in Environmental Science, University of Colorado, Boulder, Colorado.
@Current affiliation: Department of Atmospheric and Oceanic Sciences, University of Wisconsin—Madison, Madison, Wisconsin.
&Current affiliation: LightWorks, LLC., Boulder, Colorado.
Corresponding author address: Dr. Stephen A. Cohn, National Center for Atmospheric Research, P.O. Box 3000, Boulder, CO 80307-3000.
E-mail: cohn@ucar.edu
In final form 3 December 1997.

Illinois. The site was chosen because its very flat terrain eliminates the need to account for atmospheric structure and motions resulting from nonflat topography. LIFT took advantage of the presence of the Flatland96 instruments, adding three experimental lidars, a scanning Doppler radar, and additional surface instruments for the latter half of the Flatland96 campaign. The lidars, which were located at a vertex of a triangle of radar profilers, included a 2-μm Doppler lidar, a dual-wavelength backscatter lidar, and an ozone DIAL (differential absorption lidar). The distance between the radar profilers was approximately 5 km.

This report describes the LIFT field experiment and shows examples of applications for the lidar measurements collected. In section 2 we present the overall goals of LIFT and discuss motivations for the use of lidar in boundary layer research. Section 3 describes the lidars and additional instruments used in this experiment, and section 4 presents five examples of the use of LIFT measurements in boundary layer research. The final section summarizes our experience with LIFT.

2. LIFT and lidars in boundary layer research

The capabilities of the three lidars brought to LIFT allowed us to set the following measurement objectives.

1) Evaluate several terms in the boundary layer energy and ozone budgets, the time evolution of boundary layer height, surface sensible heat (temperature) flux, and surface latent heat flux.
2) Collect statistics of the vertical component of turbulent velocity including variance, skewness, and vertical coherence.
3) Estimate the fluxes of momentum and turbulence kinetic energy using the scanning lidar techniques of Eberhard et al. (1989) and Frisch et al. (1989).
4) Measure characteristics of the entrainment zone including its depth and the relation between vertical velocity and aerosol concentration.
5) Measure ozone concentration and the vertical flux of ozone aloft for comparison with in situ measurements of ozone at the surface.
6) Observe features of the shallow nocturnal boundary layer with spatial and temporal coverage only available with lidar.

A problem with calibration of the ozone DIAL has delayed analysis for the fifth objective, but analysis is under way for the other objectives.

Additional goals included instrument and technique intercomparison to better understand the strengths and limitations of new remote sensing techniques and to evaluate the performance of the new lidars. Comparisons to be made with LIFT data include

1) radial velocities from the Doppler lidar and radar wind profiler,
2) estimates of heat and momentum flux obtained by several techniques, and
3) the performance of different techniques to measure the height of the boundary layer.

Lidars are relatively new instruments for boundary layer research and have the potential to make unique observations. In recent years radar and lidar remote sensors have been used to provide a more comprehensive view of boundary layer structure and to provide spatial and temporal sampling resolution that could not be achieved with in situ sensors (Wilczak et al. 1996; Cooper et al. 1992).

There is a growing variety of types of lidar, each with different abilities. For example, a Doppler lidar can make velocity measurements in clear air with spatial and temporal resolution better than that of radar and with areal coverage of several square kilometers. In combination with a DIAL system, ozone or water vapor flux profiles can be measured through direct eddy correlation (Senff et al. 1996). Eichinger et al. (1993) describe two other lidar techniques to measure water vapor flux. Methods for using scanning Doppler lidar data to obtain turbulence parameters such as total kinetic energy and momentum flux may also be compared with each other as well as with those used by radar wind profilers. Eberhard et al. (1989) and Gal-Chen et al. (1992) discuss such methods. Long-term measured fluxes of quantities like heat, moisture, and ozone are necessary to further our understanding of interactions between the boundary layer, the earth's surface below, and the free troposphere above, and they are also needed to refine boundary layer parameterizations in models (Kiehl 1992).

Radial velocity comparison may be a key to understanding the cause of biases documented in mean vertical motion measurements from radar wind profilers (Nastrom and VanZandt 1994; Angevine 1997). Profiler winds have often been compared with rawinsondes, but lidar offers the possibility to directly

compare measured radial velocity (e.g., Mayor et al. 1997).

Lidar can complement and extend data from other measurement systems. Fast response sensors such as sonic anemometers provide long time series and can be used to measure fluxes and velocity statistics, but unlike lidar they typically are used only in the lowest few meters of the ABL. To measure mean properties, these sensors must operate for many hours as convective eddies advect past. Lidars have some of the same strengths as radar wind profilers, but they measure different quantities. Different types of lidar can measure velocity or concentrations of aerosols, ozone, or water vapor. Lidars also complement instrumented aircraft that can sample a large number of eddies in a short time but are very expensive to operate. Furthermore, profiles of turbulence statistics from aircraft require flight legs at several altitudes acquired at substantially different times. In summary, lidar strengths can include good sampling in time and space, the ability to probe well above the surface layer, moderate cost, and measurement of many quantities. Flux measurements at higher altitudes also have the advantage of representing a larger footprint and so implicitly integrate surface fluxes over a larger area (Horst and Weil 1994). Lidar measurements can be limited by the presence of optically thick clouds and precipitation or due to insufficient backscatter when "clean" (low aerosol concentration) conditions prevail.

Lidar data are uniquely suited to initialize and validate large eddy simulations (LES). For example, Avissar et al. (1998) utilize 4D volume imaging lidar data to validate an LES and Liou and Lilly (1997) use a combination of CO_2 Doppler lidar data and LES to study a CBL with a jet. Much work remains to be done in the area of validating models with lidar observations and using both tools together to better understand atmospheric processes.

3. Instruments at LIFT and Flatland96

There were three relatively new lidars present at LIFT: the 2-μm wavelength high resolution Doppler lidar (HRDL), which is capable of providing profiles of vertical velocity when staring vertically and wind speed, direction, turbulent kinetic energy, and momentum flux when scanned; the Staring Aerosol Backscatter lidar (SABL), which measures aerosol backscatter at two wavelengths and can provide detailed measurements of boundary layer height; and an ultraviolet wavelength DIAL, which measures profiles of ozone concentration and can be combined with HRDL data to derive profiles of vertical ozone flux. These lidars and supporting instruments are described below.

a. High resolution Doppler lidar

HRDL is a unique Doppler lidar that measures radial velocity as well as backscatter strength at an eyesafe wavelength. It employs coherent detection that combines a Tm:Lu YAG laser transmitter, developed at the National Oceanic and Atmospheric Administration's (NOAA) Environmental Technology Laboratory (ETL), with advanced signal processing and a high-speed hemispheric scanning system. The laser is injection seeded and diode pumped. HRDL operates at a wavelength of 2.022 μm and generates $\approx$1 mJ pulse^{-1} at a 200-Hz pulse repetition frequency. The pulsewidth is $\approx$200 ns (equivalent to a range resolution of $\approx$30 m). Signals are processed using 12 C-40 digital signal processors and are displayed in real time. The technology is described in greater detail in Grund (1996).

HRDL is typically housed in a specially modified standard shipping container (seatainer) that is convenient for shipping and for operations at sea. For LIFT the system was installed in a larger National Center for Atmospheric Research (NCAR) supplied trailer that also served as a field operations headquarters. The lidar itself is compact and lightweight, and modification for aircraft operations is planned.

Data acquired in HRDL's first field deployment suggest it can achieve simultaneously 5 cm s^{-1} velocity precision and 30-m range resolution (Grund 1997) in the marine boundary layer—about an order of magnitude improvement over prior CO_2 laser-based technologies (Mayor et al. 1997). At the time of LIFT, the laser energy had degraded considerably, reducing the signal-to-noise ratio and lowering the velocity measurement precision. We attempted to maintain a high transmit power by cooling the laser crystal, but this often resulted in condensation on the crystal, which is potentially harmful to it. As a solution, we blew dry nitrogen around the crystal to keep it dry. The laser is being redesigned to improve field performance. Despite low aerosol backscatter conditions prevailing during much of LIFT, HRDL performed well, and velocity precision during LIFT is estimated to be $\approx$25–35 cm s^{-1} for typical 1-s averages.

b. Staring aerosol backscatter lidar

SABL provides vertical profiles of aerosol backscatter with very high temporal and spatial resolution

(up to 20 Hz and 3.75 m). Aerosol concentration can be used to indicate the altitude of the top of the ABL, and SABL is also well suited for profiling through thin cirrus clouds or observing the edge of an optically thick cloud. It was designed to be compact and rugged, and it is capable of measurements from airborne, shipboard, or ground-based platforms.

SABL uses a Nd:YAG laser with a doubling crystal to transmit 15-ns pulses of green (50 mJ pulse^{-1}) and infrared (75 mJ pulse^{-1}) light at up to 60 Hz. Backscatter from atmospheric aerosols is collected by a 14-in. Cassegrain telescope and detected by a photo multiplier tube in the green channel and an avalanche photodiode in the infrared channel. These signals are digitized by two 40-MHz digitizers.

SABL has been deployed aboard an NCAR research aircraft, but LIFT was the first ground-based deployment for this instrument. A scanner assembly for SABL is planned. The instrument performed reliably during LIFT; however, a problem was uncovered with the receiver electronics for the green wavelength. A correction is being developed for the LIFT dataset and the receiver will be upgraded for future deployments.

c. UV-differential absorption lidar

The NOAA ETL ground-based ozone DIAL provides profiles of ozone concentration and aerosol backscatter from near the surface to 2–3 km above ground. Three wavelengths in the near-ultraviolet, at 266, 289, and 355 nm, are generated through upconversion and Raman shifting of the output from a flashlamp-pumped Nd:YAG laser. During LIFT, the lidar transmitter was operated at a repetition rate of 10 Hz. The atmospheric return signals of the three DIAL channels are collected with a 20-cm telescope, separated by a series of dichroic beam splitters, and then amplified with photomultipliers. The photomultiplier output is digitized at 10 MHz for 266 and 289 nm and 16 MHz for 355 nm. To collect data from near the surface to about 3 km the ozone DIAL system uses a multibeam transmitter: three lidar beams are emitted into the atmosphere at different lateral distances with respect to the receiving telescope. The 355-nm channel, which is not absorbed by ozone, provides the aerosol concentration information. The 266 and 289 wavelengths both lie within the Hartley–Huggins absorption band of ozone; 266 nm is close to the center, while 289 nm is at the wing of the absorption band. Due to their difference in ozone absorption the 266- and 289-nm pair can be used to determine ozone concentration along the lidar beam path. The DIAL technique is described further in the appendix. The fairly large separation of the 266- and 289-nm wavelength pair makes it necessary to correct for differential backscatter and extinction due to air molecules and aerosol particles. This is done by a method similar to that first used by Browell et al. (1985). Typical vertical resolution (after averaging) is 90 m for ozone concentration and 10 m for aerosol backscatter during a 30-s integration period. More information on the technical details of the ozone DIAL can be found in Zhao et al. (1994).

Preliminary analysis of the DIAL data from LIFT has revealed systematic errors in the derived ozone profiles in the lowest 1 km. The multibeam transmitter design of this lidar requires calibration measurements to correct for changing overlap between the three transmitted beams and the field of view of the receiving telescope in the lower part of the measurement range. Apparently, during the LIFT campaign, characteristics of the transmitter changed enough between calibration measurements to cause these systematic errors in the ozone profiles. Depending on the timescale of system parameter drifts, the ozone concentration fluctuation measurements needed for the eddy correlation flux retrieval may also be subject to systematic errors. Currently we are investigating possible data correction schemes prior to the flux retrieval and we are assessing the remaining errors in the flux estimates due to system parameter drifts. We are also exploring methods to stabilize the beam overlap for future experiments.

d. Additional instruments

In addition to the three lidars, Flatland96 and LIFT included supporting measurements from a scanning 3-cm wavelength Doppler radar (Wurman et al. 1995), a triangle of UHF boundary layer wind profilers of the type described by Carter et al. (1995), three Flux-PAM surface measurement stations (Militzer et al. 1995), and a series of Cross-Chain Loran Atmospheric Sounding System (CLASS) rawinsonde soundings (Lauritsen et al. 1987).

The 3-cm wavelength Doppler on Wheels (DOW1) weather radar was used to observe the mesoscale convective structure around the LIFT site. This radar, which is a mobile, pulsed Doppler radar, was collocated with the lidars. Its beamwidth is ≈1.2° and the gate spacing used was nominally 75 m. DOW1 was primarily operated in surveillance mode (scanning in azimuth with a fixed elevation angle) to provide information on both the boundary layer and deep con-

vection within 25 km of the LIFT site. The larger-scale convective structure was obtained from *GOES-8* satellite imagery. Visible and infrared images were archived every 15 min (visible images during the daytime only) throughout the project.

Positioning of the three wind profilers is described in Angevine et al. (1998). One profiler (part of an NCAR Integrated Sounding System; see Parsons et al. 1994) was collocated with the LIFT site. These 915-MHz radars were usually configured to provide a wind and virtual temperature profile every 30 min. Backscatter strength, proportional to the refractive index structure parameter C_n^2, can provide a signature (local maximum) at the boundary layer top and can be used to measure boundary layer height z_i. The profiler scan sequence used all four oblique beams, making the dataset suitable for measurement of momentum flux (e.g., Shaw and Zhong 1994). During limited periods the profiler beam pointing sequence was followed by HRDL (limited to the five available profiler pointing directions) to evaluate the relative performance of these instruments. There were also several periods of continuous vertical staring, which provided vertical velocity variance at the expense of horizontal winds and also periods of continuous temperature profiling, from which direct vertical temperature flux may be measured (Angevine et al. 1994). Measurements from surface meteorological stations and approximately 100 CLASS rawinsondes are also available from Flatland96 to provide context for the lidar measurements.

4. Data and science examples

The LIFT experiment took place from 26 July to 22 August 1996. Data were collected only on days with good anticipated CBL development. A typical day started before sunrise by operating the Doppler lidar in a shallow elevation or azimuth scan mode to study the nocturnal and transitional boundary layer. This provided vertical cross sections of radial air motion that often showed nocturnal low-level jets. Elevation scans were generally oriented along and across the mean wind direction, showing details of the streamwise and cross-stream wind components and their turbulent fluctuations. Forty-six hours of data were collected in this mode. After sunrise, shallow mixing could be seen in the scans. Shallow scans were continued until midmorning when the mixed layer rose above the Doppler lidar's minimum range of ≈350 m. At this time, HRDL was either pointed vertically to study fluxes and velocity statistics (110 h), or repeated azimuth scans were begun for turbulence parameter and momentum flux measurement (47 h). Uninterrupted vertical pointing or azimuth scanning was typically continued until after sunset. Ten hours of instrument comparison scans (following the profiler beam sequence) and several hours of volume scans were also collected to compare radar and lidar system performance.

The LIFT dataset contains 12 days when the Doppler lidar pointed vertically all day and 4 days of continuous azimuth scans. SABL was turned on each morning around 0600–0800 LT and data were collected in a continuous vertical mode until sunset. The DIAL, which also pointed vertically, was operated on most of the 12 "vertical days" and more than 160 h of DIAL data were collected. Although the CBL was the main focus of LIFT, many other interesting phenomena were observed, including a gust front, waves, cirrus, and the morning and evening boundary layer transitions. Data were also collected for one continuous 36-h period.

a. Application of the HRDL vertical velocity data

By pointing the Doppler lidar directly overhead we can measure vertical velocity ω every 30 m in altitude from the minimum range of the lidar (about 350 m) to the top of the CBL. The temporal resolution of the measurement depends on the signal-to-noise ratio (SNR), which is a function of aerosol concentration. On most days the SNR was large enough to obtain a measurement every second. Occasionally, very clean days with low aerosol concentration required as much as 5 or more seconds of integration to obtain useful data. During the experiment HRDL was usually operated with the beam in a fixed vertical position, typically from midmorning, when the mixed layer rose above the lidar's minimum range, until sunset. The spatial and temporal resolution of this data, and the number of hours of boundary layer observations, make this a unique dataset.

Time–height displays of vertical motion, such as Fig. 1, reveal thermals advecting past the lidar and occasionally show their relationship to cumulus clouds. Updrafts and downdrafts can pass over the site in less than 1 min on windy days and may take as long as 15 min on calmer days. Windy days allow sampling of a larger cross section of the atmosphere in the same time interval, leading to more representative regional measurements. We also notice a high degree of vertical coherence in the data. Thermals (or plumes) in the

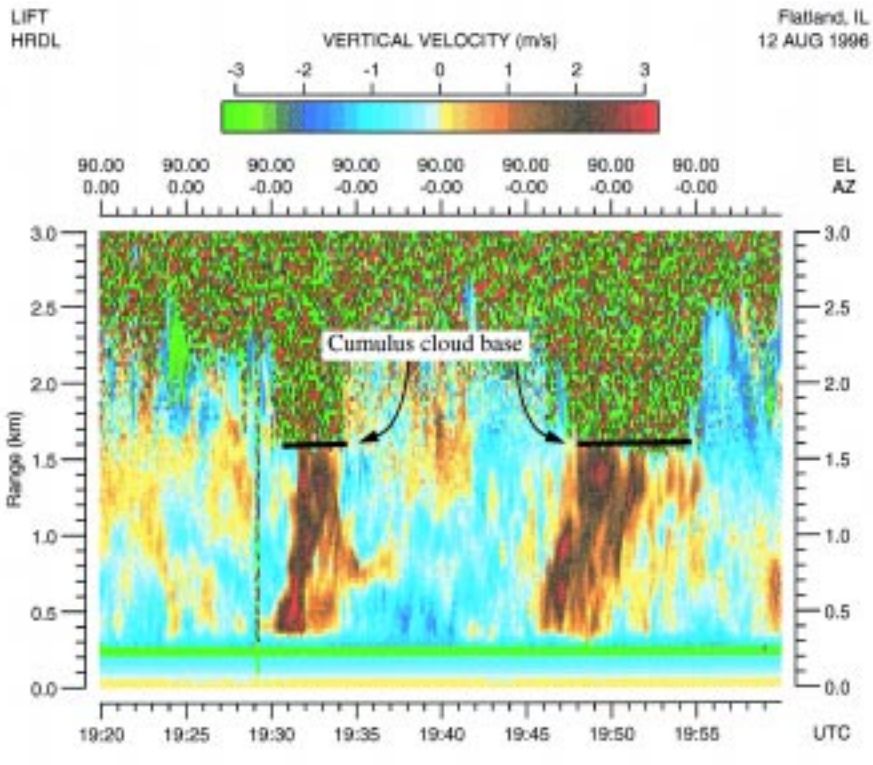

FIG. 1. Time–height display of vertical velocities from the 2-μm Doppler lidar. The width of the image is 40 min and the height is 3.0 km. Two large updrafts can be seen, one from 1930 to 1935 UTC and another from 1945 to 1952 UTC, which feed into the cumulus cloud bases near 1500 m.

mixed layer often extend from the minimum range of the Doppler lidar to the top of the CBL. When combined with backscatter data from SABL, the ω data will be used for detailed studies of the motion in the vicinity of the entrainment zone.

Figure 2 shows an example of ω at 750 m above ground level (AGL) from 1200 to 1400 LT on 2 August 1996. The temporal resolution of this time series is 2 s. A quantization limit of 20 cm s^{-1} was imposed by the lidar data system, but this limit will be removed for future experiments. Calculations of profiles of mean vertical velocity $\overline{\omega}$ over 3-h time spans sometimes reveal a bias, with $\overline{\omega}$ nearly constant with altitude but varying between −0.5 and 0.25 m s^{-1} for different time spans. We expect $\overline{\omega} \approx 0$ for long time averages. Data from radar wind profilers located at and near HRDL are available for comparison. Figure 3 compares vertical velocity measured with HRDL with that from the collocated wind profiler (30-s resolution). Both instruments were staring vertically and both see similar features. This data will be used to investigate velocity biases. Fortunately, if the nonzero mean is a systematic error it will not preclude use of the data for studies of turbulent fluxes and higher-order moments of ω.

The variance σ^2 of a time series contains contributions from both uncorrelated and correlated fluctuations. We use autocovariance functions (ACF) of the ω time series to separate atmospheric variability from measurement variability (e.g., Mayor 1995). Figure 4 shows an estimate of the vertical velocity variance σ_ω^2 as a function of height (dots) for the same 2-h period as Fig. 2. The total variance of each time series (solid line), which includes uncorrelated variance from instrumental and atmospheric noise, is also shown. Error bars on σ_ω^2 were computed using the integral scale of the time series following Lenschow et al. (1994). The error bars are of order 30%. The integral scale was determined at each altitude by noting the lag at which the ACF first becomes ≤ 0. For this series the integral scale was about 90 s. The shape of the variance profile agrees well with earlier observations, shown for example, in Stull (1988). For the time series of Fig. 2, σ_ω^2 was approximately 0.91 $m^2 s^{-2}$ and the uncorrelated variance was 0.25 $m^2 s^{-2}$.

Turbulent virtual heat flux is defined as $Q_v = \rho C_p \overline{\omega}$. This direct definition requires a measurement of both

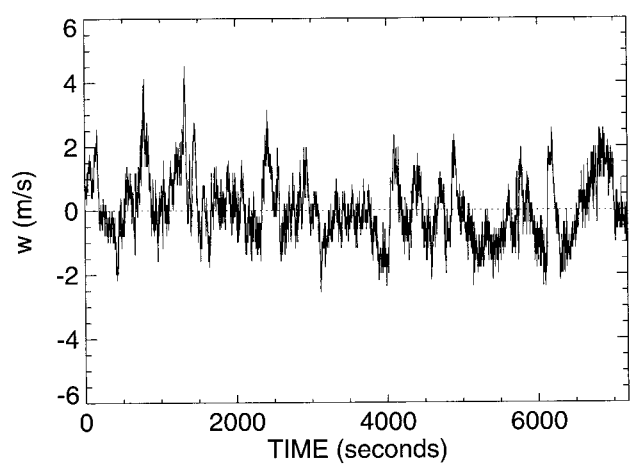

FIG. 2. Vertical velocities measured with HRDL at 2-s averaging, collected from 1200 to 1400 LT at 750 m AGL on 2 August 1996.

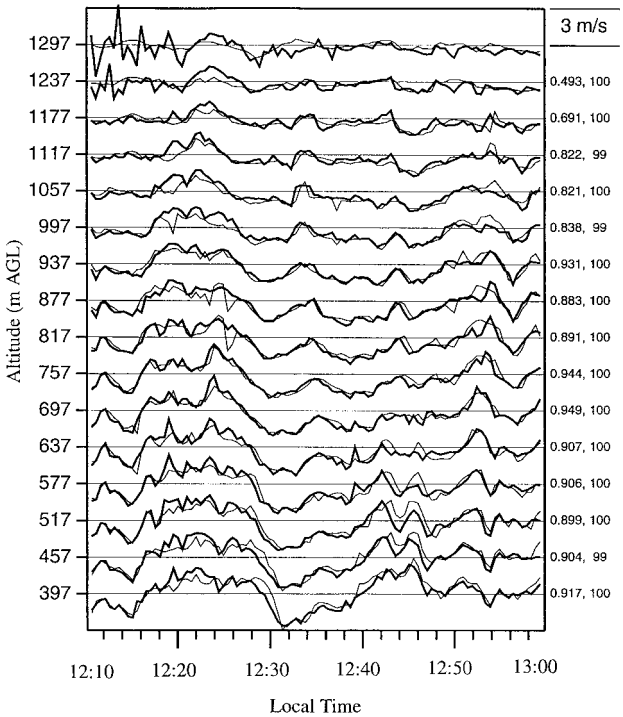

FIG. 3. Vertical velocity measured with HRDL (thick) and the wind profiler (thin) over 50 min on 6 August between 400 and 1300 m AGL. HRDL data was averaged to 30 s to match the profiler dwell time. Each altitude represents a velocity interval of 3 m s^{-1}. Columns at right are the correlation between the two instruments and the number of points available for comparison at that altitude.

ω and virtual potential temperature θ_v simultaneously, so that their covariance $\overline{\omega' \theta_v'}$ can be calculated. However, following a method described by Angevine et al. (1994) using radar measurements we can use σ_ω^2 data from the Doppler lidar to indirectly estimate the surface virtual heat flux Q_{vs}. This indirect method uses an empirical relationship between the remotely measured σ_ω^2 and the convective velocity ω_* in CBLs, $\sigma_\omega^2 \approx \beta\omega_*^2$. Eilts et al. (1987) using radars have found that β ranges from about 0.39 to 0.52 within $0.2 < z/z_i < 0.5$. The technique also requires a measurement of mixed-layer height z_i and mean surface virtual temperature $\overline{T_{vs}}$, which can be determined from the lidar and surface in situ sensors, respectively. For our case, $\overline{z_i}$ was ≈1100 m AGL and $\overline{T_{vs}}$ was 23°C. Using a measured σ_ω^2 = 1.1 m^2 s^{-2} (from the profile in Fig. 4 between 400 and 500 m, which corresponds to 0.31 to 0.38 z/z_i) and taking β = 0.5, we estimate Q_{vs} = 110 W m^{-2}.

The Q_{vs} was also estimated using measurements from a Flux-PAM station, which provided a value of $\overline{\omega' \theta'}$ = 0.08 m K s^{-1}. This was used in the direct

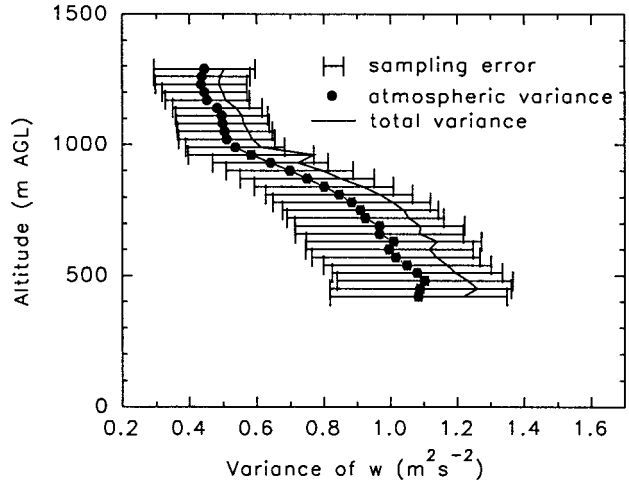

FIG. 4. Profile of HRDL vertical velocity variance (dots) with error estimates for the same time period as Fig. 2. The solid curve includes variance due to uncorrelated measurement noise.

definition to yield Q_{vs} = 99 W m^{-2}. Our result compares well with this surface measurement. An advantage of the indirect method, using remotely sensed data aloft, is that it is more representative of the average surface virtual heat flux over heterogeneous terrain, compared with the direct method at a single surface point.

We have computed the skewness of ω, shown in Fig. 5. Skewness (the normalized third moment of a distribution) is a measure of asymmetry around the mean. Data from the 2-h period show skewness increasing with altitude and sampling errors ranging from 0.2 (100%) at 400 m to 0.4 (35%) at 1100 m. Positive values of ω skewness at all altitudes are con-

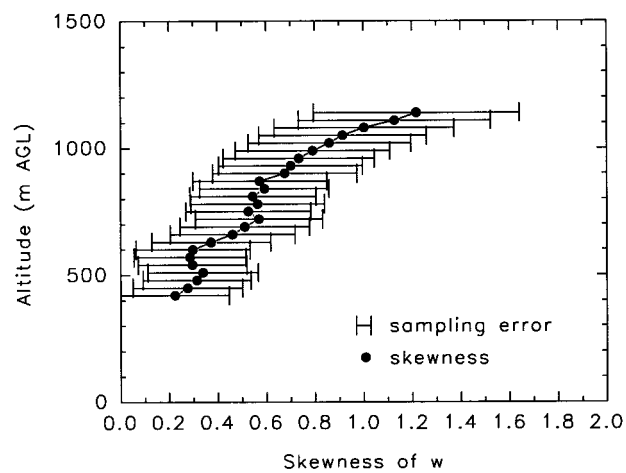

FIG. 5. Profile of HRDL vertical velocity skewness (dots) and sampling error for the same time period as Fig. 2.

sistent with previous aircraft and lidar observations (LeMone 1990; Lenschow et al. 1994; Gal-Chen et al. 1992), numerical modeling results (Moeng and Rotunno 1990), and the concept that thermals with strong updrafts cover a smaller area of the mixed layer than the compensating, weaker downdrafts.

b. Measurement of CBL depth from lidar and radar backscatter

The height of the base of the inversion layer that caps the convective boundary layer, z_i, is a fundamental measurement for boundary layer research. It is an important length scale in parameterizations of boundary layer quantities, such as fluxes and vertical gradients of wind, potential temperature, and moisture. Variances and higher-order moments of vertical velocity also scale with z_i (Stull 1988), and it is also used in deriving quantities such as heat flux and entrainment velocity. Using the LIFT dataset we can find z_i independently using backscatter from SABL, HRDL, or the UHF wind profilers. We will use this dataset to compare the different measurements and different analysis techniques.

The free atmosphere above the boundary layer is separated from the mixed layer by the entrainment zone. This zone can be defined as that region where the buoyancy flux $\overline{\omega' \theta'}$ is negative. Since $\overline{\omega' \theta'}$ is not easily measured, an alternate definition is sometimes used: that region where more than 5% and less than 100% of air on a horizontal plane has free atmosphere characteristics (e.g., Deardorff et al. 1980). Area averaging is required by the definition because a mean height is desired rather than the height up to which local thermal plumes rise or down to which free atmosphere air is entrained. This entrainment zone can have a thickness of several hundred meters and so can contain a significant fraction of the total boundary layer. The z_i can be defined as the height at which $\overline{\omega' \theta'}$ has its minimum or where 50% of the air has free atmosphere characteristics.

Lidar backscatter is well suited to the latter measurement. Aerosols generated at the surface are often well distributed throughout the daytime mixed layer, with their concentration sharply decreasing through the entrainment zone. So a gradient in backscatter from HRDL or either SABL wavelength can be used to indicate z_i.

Backscatter from the UHF boundary layer wind profiler can also be used to find z_i. The reflectivity of these profilers in clear air is proportional to the refractive index structure constant, which is a strong function of humidity gradients. Angevine et al. (1994) and others have used a peak in reflectivity to infer z_i, though it is not clear that this peak (maximum humidity gradient) will occur at the same altitude as z_i indicated by aerosol concentration. This will be tested with the LIFT dataset.

Figure 6 shows the backscatter strength from SABL (1064-nm channel) (top) and the wind profiler (bottom) for a 2-h period. SABL data has a strong reflectivity gradient varying between 400 and 700 m and shows the tops of thermal plumes advected past the lidar. The profiler data, which has less time resolution, shows a clear peak (not gradient) in reflectivity at about the same height as the lidar gradient. The fine-resolution lidar data can also be used to study entrainment processes.

As an objective way to identify features of the backscatter profiles we have used a wavelet transform technique to identify the slope in the SABL backscatter at 1-min resolution and to find the profiler reflectivity peak averaged to 10-min resolution. This technique is described in Cohn et al. (1997) and Mann et al. (1995). Figure 7 compares z_i from these instruments. In this figure, averaged SABL backscatter profiles are also plotted every 10 min (the very strong backscatter at 1000 LT is from a cloud). The z_i should be at the center of the backscatter gradients. The lidar (thick horizontal curve) and radar (thin horizontal stepped curve) estimates of z_i agree well with each other and appear to be near the center of the entrainment zone. HRDL results for the same time (not shown) are similar to those from SABL. Differences occur near clouds and during the early part of the 2-h period when the boundary layer was shallow.

The LIFT dataset has many days on which wavelet and other methods to determine z_i can be tested. In addition, rawinsonde measurements of z_i and ceilometer measurements of the height of cloud base can support these measurements.

c. Comparison of HRDL and DOW Doppler data

The scanning Doppler weather radar, DOW1, measured radial velocity in the clear-air boundary layer. This mesoscale view was useful in determining the type of convection present (i.e., linear, cellular, or unorganized). Weckwerth et al. (1997) demonstrate the power of using Doppler lidar and radar to measure both mesoscale and microscale motions simultaneously.

Most of the days on which DOW1 was operating during LIFT, it provided surveillance (varying azi-

muth) scans of the area surrounding the lidars. While in surveillance mode on 7 August 1996, DOW1 observed a gust front propagating toward the lidar site. The DOW1 velocity field displayed in Fig. 8a shows the gust front located approximately 3 km from the radar at 1530 LT (2130 UTC) denoted by black arrows. The fine line of enhanced radar reflectivity (Fig. 8b) corresponds to an area of convergence in the velocity field. At this time, HRDL began performing elevation scans through the approaching gust front at 355° azimuth. In these scans (Fig. 8c) the elevated layer of strong velocities (blue) is due to cold air outflow and winds near the surface being slowed by frictional effects (e.g., Wakimoto 1982). There is a suggestion of a wave pattern occurring atop the cold pool, which may be an indication of Kelvin–Helmholtz instability. As the gust front propagated past the site, elevation scans were taken at 180° azimuth (Fig. 8d). At this later time (1550 LT), the elevated layer of relatively stronger flow is still apparent but the flow atop the cold pool seems to be more laminar. The detailed finescale structure available from HRDL and the larger-scale view obtained from DOW1 provide different and complementary views of this gust front.

During LIFT, the larger-scale view of convection observed by DOW1 provided information that was not available with the lidars alone. In their typical vertical staring mode, the lidars would probably not have noticed the passage of the gust front. This is clear from

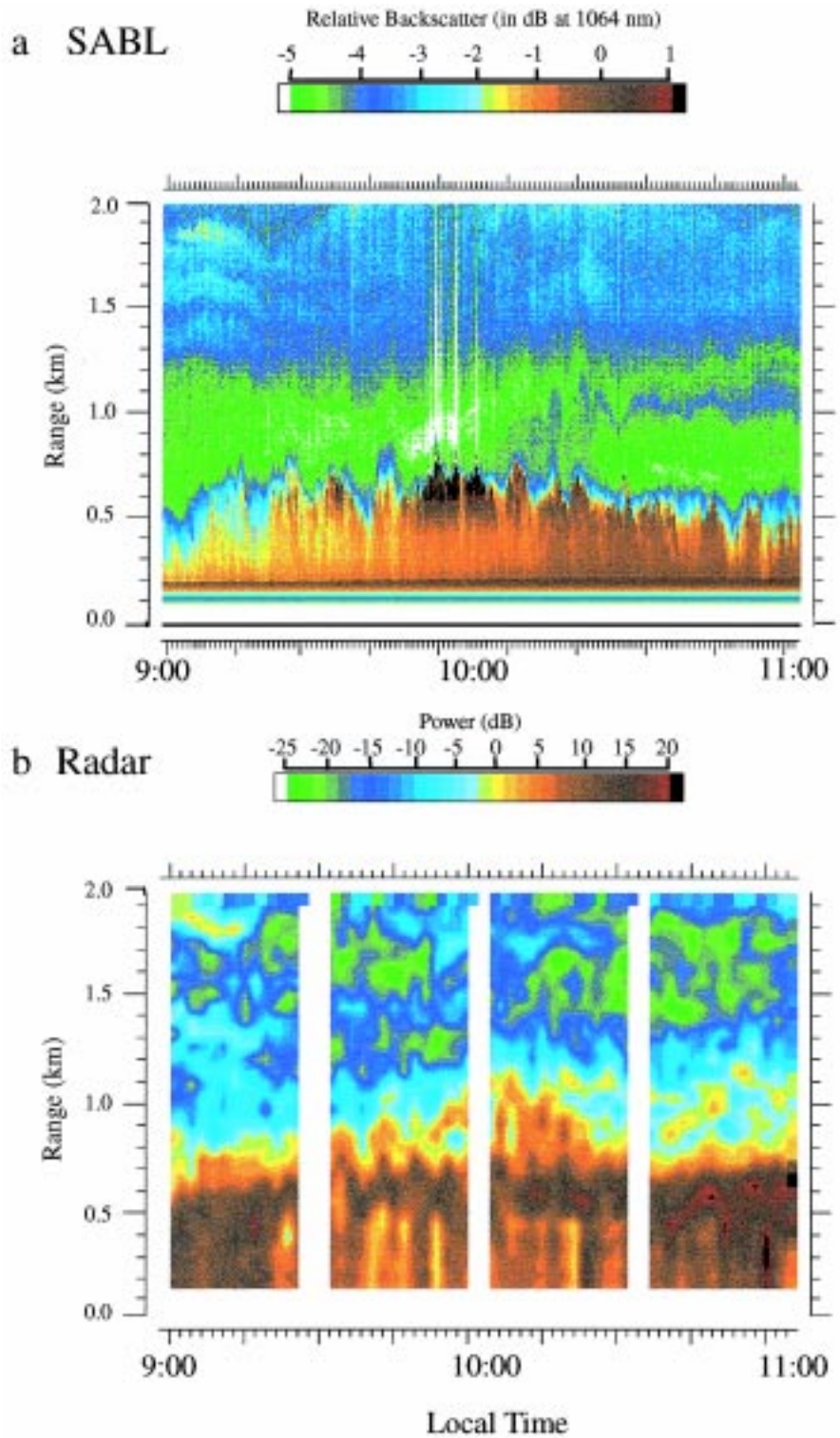

FIG. 6. (a) Time–height cross section (0900 to 1100 LT on 20 August 1996) of SABL backscatter strength (1064-nm channel) showing a strong gradient at the height of the entrainment zone. The strongest backscatter (black) is from a small cloud. (b) Wind profiler relative power for the same time period. The maximum signal occurs from strong moisture gradients near the boundary layer top. Missing data on the hour and half-hour occurs during radio acoustic temperature sounding (RASS).

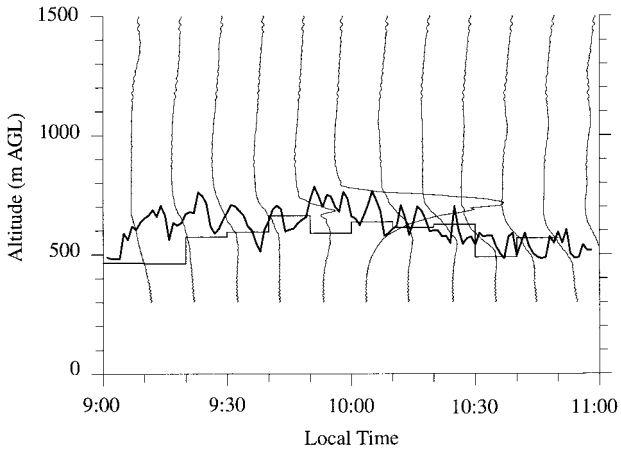

FIG. 7. The z_i measured with a wavelet transform method from SABL 1-min reflectivity profiles (thick horizontal line), and wind profiler 30-min profiles (thin stepped line). Vertical profiles of SABL backscatter strength (10-min average) are also shown (see text for details). Both SABL and profiler z_i are near the gradient in backscatter.

the backscatter signal observed by SABL during gust front passage (Fig. 9). In this time series of the backscatter in the infrared channel, the only indication of the gust front passage was a short enhancement in backscatter at 1545 LT (2145 UTC), likely due to the gust front lifting dust at its leading edge.

d. Nocturnal and transitional BL observations with HRDL

Observations of the nocturnal, or stable, boundary layer (SBL) and the overlying residual layer, during morning and evening transitional periods, are not as common as observations of the daytime CBL. In the evening, when surface heating ceases, a stable layer forms just above the earth's surface, which can impede the turbulent connection between the surface and free atmosphere that existed previously. Mixing then only occurs when the wind shear is large enough to overcome the thermal stratification. The result is that turbulence is often episodic or intermittent (Mahrt and Gamage 1987). The decay of convective turbulence in the residual layer has been studied by Nieuwstadt and Brost (1986) using an LES, but observational data are rare.

Another result of the decoupling between the surface and residual layer is the formation of low-level jets (LLJ). These occur frequently over much of the midwestern United States, generally forming a few hundred meters above the surface (Blackadar 1957; Whiteman et al. 1997). Because LLJs can transport a tremendous amount of air horizontally very quickly, they are important in thunderstorm initiation and pollution transport (Stensrud 1996).

Although LIFT was aimed at studying the CBL, we took advantage of the deployment and collected SBL data often. For example, on several mornings Doppler lidar data collection began hours before dawn and continued for hours after sunset. On one occasion, the Doppler lidar was operated continuously overnight. Although HRDL does not possess the long-range capabilities of radars, it excels in providing the near-surface observations and height resolution required for SBL research because of the small beam diameter and complete absence of sidelobes.

An example of the predawn SBL and subsequent transitional period data is shown in Fig. 10. The top panel elevation scan shows a well-developed nocturnal jet (red) prior to the onset of surface heating on 6 August 1996. This scan was taken pointing north along the mean southerly jet-level wind direction. There was little turning of the wind with height within 500 m of the surface. The 1500 UTC surface analysis showed that the experiment site was dominated by a region of loosely packed isobars west of a high centered over Delaware. Winds veered with height, suggesting warm air advection. Satellite images and local observations show regionally clear conditions, and there were no significant radar echoes within 150 km. During LIFT, several jet episodes were observed in the early morning and through the onset and development of the CBL. Well-defined jets were frequently observed below 150 m, closer to the ground than commonly reported, although Sisterson and Frenzen (1978) have reported such jets.

Because it is possible with HRDL to resolve both the jet and the fine details of the wind field very close to the surface, it is feasible to study the details of the diurnal formation and breakup of LLJs, and the effect of entrained jet momentum on the growing convective boundary layer. The middle and lower panels of Fig. 10 show two stages in the evolution of the CBL from the SBL. The middle scan was taken just after the onset of surface heating. Convective plumes are seen as low velocity structures (green) extending up from the surface. Intermediate scans documented progressive erosion of the jet as the CBL begins to form. At this time, the plumes appear to be about 100 m wide with a 1:1 aspect ratio. In the bottom scan taken 47 min later, the CBL is well defined and the convective activity has completely eroded the jet. The plumes have grown to 250-m height, while the apparent plume aspect ratio remains near 1:1. An azimuth scan at 1° el-

evation (not shown) taken at about this time suggested that the plumes were organized into horizontal convective rolls aligned approximately with the mean wind direction. After this time HRDL began continuous vertical profile operation to observe development of the CBL. Further investigation into the interaction between jets and formation of convective structures is in progress.

e. Ozone flux

Although the ozone DIAL data has not been analyzed because of the calibration problem discussed in section 3c, deployment of this instrument was a large part of LIFT. The primary goal of deploying this lidar was to study the vertical turbulent flux of ozone in the summertime convective boundary layer. By combining the highly resolved ozone DIAL data with vertical wind speed data collected with HRDL, ozone flux profiles can be retrieved using the eddy correlation technique. Using a DIAL–Doppler lidar combination to remotely measure constituent fluxes has been successfully demonstrated in previous studies, for example, by Senff et al. (1996). The LIFT campaign offered the opportunity to evaluate the potential of this new technique for long-term, routine flux measurements under varying meteorological conditions. Also, ozone fluxes at the surface and entrainment zone can be estimated from the DIAL ozone variance profiles by making use of a flux-variance similarity relationship analogous to the method applied to water vapor DIAL data by Kiemle et al. (1998).

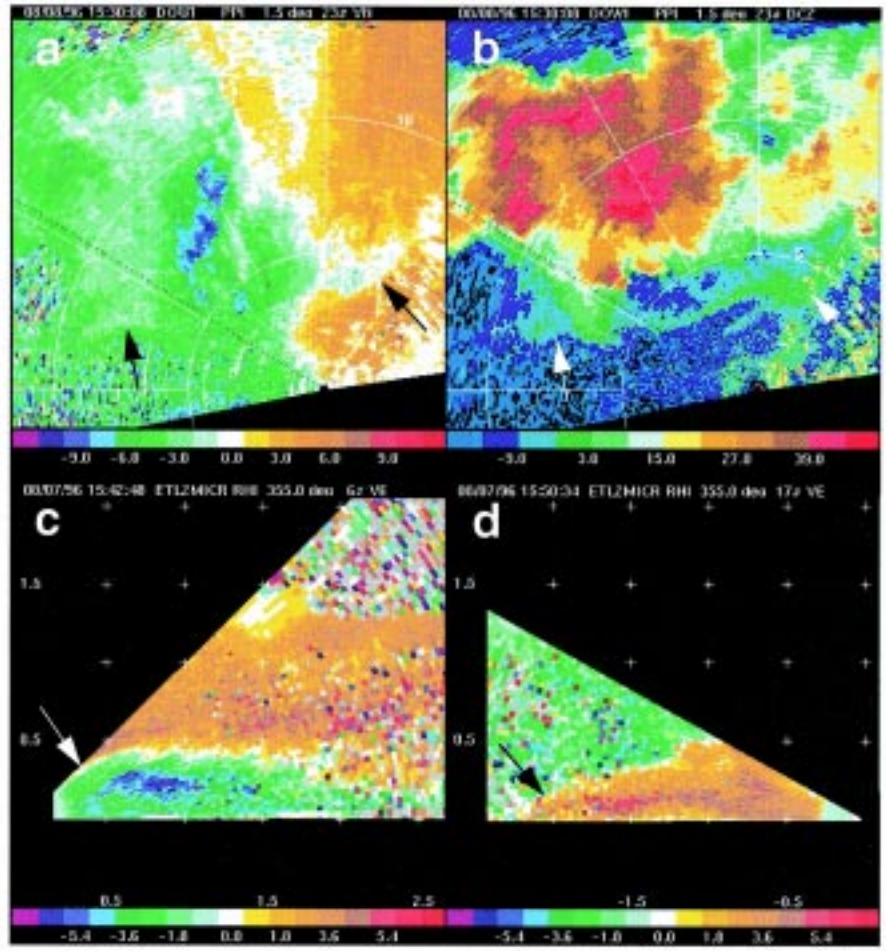

FIG. 8. Data from a gust front propagating over the LIFT site on 7 August 1996 at 1545 LT. Doppler velocities from DOW1 (m s^{-1}) are shown in (a) while the corresponding reflectivities (dBZ_e) are shown in (b). Range rings in (a) and (b) are every 5 km. The HRDL radial velocities normal to the gust front's approach and retreat are shown in (c) and (d), respectively. Tic marks are every 500 m. Arrows depict the locations of the gust front.

5. Summary

The LIFT experiment produced a high quality dataset from two unique lidars, three wind profilers, a portable weather radar, and supporting in situ instruments. Due to a calibration problem, the data collected with a third lidar (the ozone DIAL) are subject to significant systematic errors. We are currently assessing the impact of these errors on our ability to retrieve ozone profiles and fluxes from the DIAL data. The LIFT dataset can be used to study many characteristics of the boundary layer including its evolution from a nocturnal stable boundary layer through a daytime convective boundary layer. The dataset can be used to explore the capabilities of these lidars and of lidar technology in general when applied to boundary layer research. Lidar performance and the performance of techniques to measure fluxes of heat, moisture, and momentum can also be studied.

We have presented examples showing initial application of these data to measurement of velocity statistics and heat flux, observation of the boundary layer

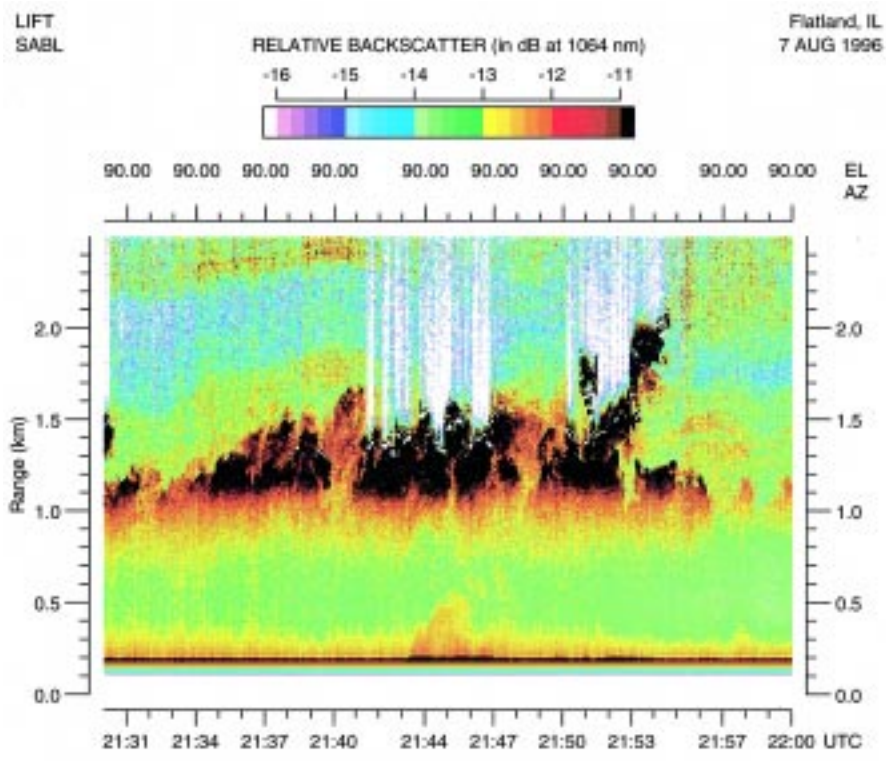

FIG. 9. Time–height cross section of infrared SABL backscatter on 7 August 1995 from 2130 to 2200 UTC (1530 to 1600 LT). The blip at 2145 UTC (1545 LT) below 500 m was caused by the gust frontal passage.

height at high time resolution, observation of a gust front, and observation of features of shallow low-level jets in the nocturnal boundary layer.

From a fixed location on the ground, adequate sampling of ω for area-averaged fluxes and other turbulence statistics depends mostly on the mean horizontal wind advecting a representative sample of eddies over the lidar. In the future, sampling from moving platforms, such as trucks and airplanes, should provide measurements with lower sampling error. Plans for future analysis of the ω data include determining the cause of the nonzero mean, calculating two-point turbulence statistics, and similarity scaling of the higher-order moments of ω. Related activities will include comparing the ω measurements with those from a radar wind profiler and investigating cloud processing of aerosols.

Acknowledgments. The LIFT project was funded by the NCAR Atmospheric Technology Division Director's Office and the Department of Energy/OAGR. We appreciate the help of the University of Illinois with siting and logistics, and of technical support staff from NCAR and NOAA including H. Avila, J. Daughenbaugh, C. Frush, C. Walther, M. Susedik, M. Randall, W. O. J. Brown, R. Richter, J. George, K. Koenig, R. Marchbanks, Y. Zhao, C. Locker, and J. Intrieri. Initial partial funding for HRDL was provided by W. Bach under Army Research Office Contract ARO 117-92. Development of the scanner, adaption of HRDL for marine operations, and shipboard measurements were made possible under Office of Naval Research Grant N00014-93-F-0029. The DOW1 was provided by the Joint Mobile Research Facility, sponsored jointly by the University of Oklahoma, the National Severe Storms Laboratory, and NCAR, through the assistance of J. Wurman. We benefited greatly from the guidance of D. Lenschow, R. Doviak, D. Parsons, S. Oncley, M. Hardesty, R. Banta, V. Wulfmeyer, and J. Keeler. Finally, LIFT would not have been possible without the flexibility and support of the Flatland96 investigators, in particular W. Angevine.

Appendix: Brief lidar tutorial

Techniques for lidar (light detection and ranging) remote sensing of the atmosphere have seen steady evolution paralleling technological advances in optics, signal processing, and lasers, and they have become important tools for atmospheric research. Many lidar techniques have been developed to measure scattering properties, chemical composition, thermodynamic characteristics, and velocity. Although the number of lidars used for atmospheric research is rapidly increasing, they are still relatively rare and the lidar field is specialized. To aid the reader who may be unfamiliar with lidar, the operating principles employed by the three state-of-the-art lidars deployed at LIFT are described below. A more comprehensive description of lidar remote sensing can be found in Measures (1984).

A typical modern backscatter lidar transmits a short pulse of laser light and records the time history of the scattered light intensity received by a telescope and optical detector. The return signal represents the scattering from aerosols, cloud particles, and molecules (Rayleigh scattering is important for wavelengths less than ≈ 1 μm). Between the lidar and the scattering range, the light pulse is subject to attenuation because of scattering and absorption by aerosols and molecules. Thus, the lidar signal from each range depends on the scattering properties at that range as

well as properties over the path traveled, so quantitative evaluation of atmospheric optical properties can be complicated. Several advanced techniques have been developed for calibrated retrievals (Grund and Eloranta 1991; Ansmann et al. 1992; Eloranta and Forrest 1986; Kovalev 1993). However, when atmospheric attenuation and scattering are small, simple lidar backscatter data may be easily interpreted to reveal atmospheric structure. SABL is a simple backscatter lidar that simultaneously acquires backscatter profiles at 1064 and 532 nm and has the relatively fine-range resolution needed to show detailed atmospheric structure. Two important distinctions between lidar and radar wind profilers are that lidars have very narrow beam profiles without sidelobes so that observations arbitrarily near the ground or other obstacles can be made and that because lidars operate at short optical wavelengths, they respond largely to atmospheric aerosols rather than seeds, insects, or moisture and temperature inhomogeneities. Thus, lidars may be run side by side without interference and, for eye-safe lidars, there are no special restrictions, frequency allocations, or licensing requirements.

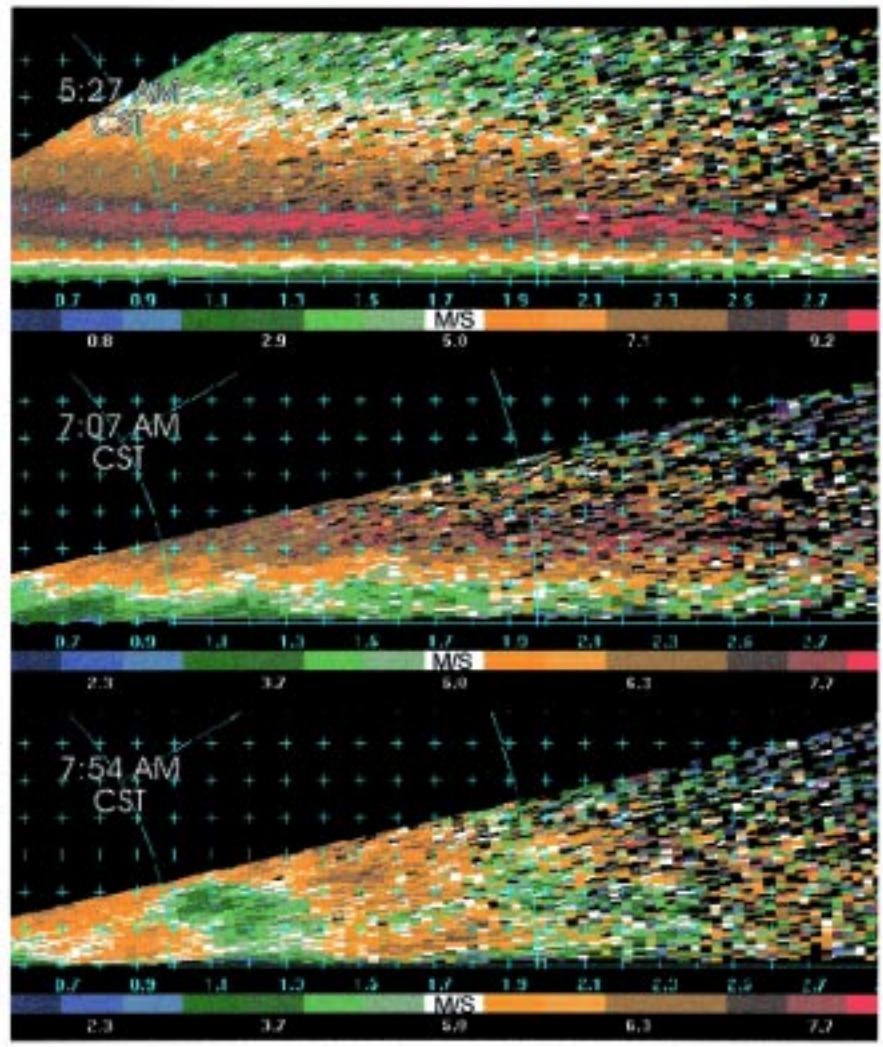

FIG. 10. HRDL shallow elevation scans showing the transition from a stable, nocturnal BL to a convective BL. The top panel shows a well-developed low-level jet; the middle panel shows the initial development of convective plumes shortly after onset of surface heating; the lower panel shows well-developed plumes that have eroded the nocturnal jet.

Differential absorption lidars, such as the ozone DIAL system deployed at LIFT, provide a measure of concentrations of chemical species making use of the *attenuation* of the lidar signal due to absorption by these chemical species. DIAL systems operate alternately or simultaneously on at least two wavelengths. One is chosen to match an absorption line of the species of interest while another, nearby wavelength, is chosen to be relatively free of attenuation by that species. If the on- and off-line wavelengths are sufficiently close, the backscatter and attenuation due to aerosol is essentially the same for both. But when the chemical species of interest is present the on-line wavelength will be subject to additional attenuation and the on-line signal return will show an increasing deficit with range when compared to the off-line return. Thus, the species concentration can be calculated from the relative slopes with range of the on-line to off-line signals. DIAL measurement accuracy is largely a function of the knowledge of the absorption line profile, the relative range-dependent response of the lidar between the on- and off-line wavelengths, and any differences in the attenuation due to aerosols or other species between the two wavelengths.

In addition to backscatter intensity, Doppler lidar measures the backscattered light frequency relative to the transmitted light frequency as a function of range. Since suspended aerosols are moving with the atmo-

sphere within the scattering volume, radial velocity can be calculated using the Doppler equation. In a Doppler lidar, range resolution and velocity resolution are competing performance specifications because the shorter the laser pulse (the better the range resolution), the broader the frequency spectrum associated with that pulse. It therefore becomes increasingly difficult to determine with a specified accuracy the peak of the Doppler spectrum in the presence of noise as the range resolution is increased. The solution employed in HRDL is to shift the laser operating wavelength from the traditional 10.6-μm CO_2 laser wavelength (e.g., Post and Cupp 1993) to as short a wavelength as feasible consistent with eye-safe operations by employing a newly developed laser and to operate at a high pulse repetition rate so the returns from many pulses may be averaged in a short time to provide the SNR needed for accurate velocity determination. Velocity errors are primarily a function of SNR and the accuracy of the determination of the transmitted pulse frequency.

References

Angevine, W. M., 1997: Errors in mean vertical velocities measured by boundary layer wind profilers. *J. Atmos. Oceanic Technol.,* **14,** 565–569.

——, R. J. Doviak, and Z. Sorbjan, 1994: Remote sensing of vertical velocity variance and surface heat flux in a convective boundary layer. *J. Appl. Meteor.,* **33,** 977–983.

——, A. W. Grimsdell, J. M. Warnock, W. L. Clark, and A. C. Delany, 1998: The Flatland Boundary Layer Experiments. *Bull. Amer. Meteor. Soc.,* **79,** 419–431.

Ansmann, A., U. Wandinger, M. Riebesell, C. Weitkamp, and W. Michaelis, 1992: Independent measurement of extinction and backscatter profiles in cirrus clouds by using a combined Raman elastic-backscatter lidar. *Appl. Opt.,* **31,** 7113–7131.

Avissar, R., E. W. Eloranta, K. Gurer, and G. J. Tripoli, 1998: An evaluation of the large-eddy simulation option of the regional atmospheric modeling system in simulating a convective boundary layer: A FIFE case study. *J. Atmos. Sci.,* **55,** 1109–1130.

Blackadar, A. K., 1957: Boundary layer wind maxima and their significance for the growth of nocturnal inversions. *Bull. Amer. Meteor. Soc.,* **38,** 283–290.

Browell, E. V., S. Ismail, and S. T. Shipley, 1985: Ultraviolet DIAL measurements of O_3 profiles in regions of spatially inhomogeneous aerosols. *Appl. Opt.,* **24,** 2827–2836.

Carter, D. A., K. S. Gage, W. L. Ecklund, W. M. Angevine, P. E. Johnston, A. C. Riddle, J. Wilson, and C. R. Wilson, 1995: Developments in UHF lower tropospheric wind profiling at NOAA's Aeronomy Laboratory. *Radio Sci.,* **30,** 977–1001.

Cohn, S. A., C. J. Grund, S. D. Mayor, and W. M. Angevine, 1997: Boundary layer height and vertical velocity measurements at LIFT. Preprints, *12th Symp. on Boundary Layers and Turbulence,* Vancouver, BC, Canada, Amer. Meteor. Soc., 7–8.

Cooper, D. I., W. E. Eichinger, D. B. Holtkamp, R. R. Karl Jr., C. R. Quick, W. Dugas, and L. Hipps, 1992: Spatial variability of water vapor turbulent transfer within the boundary layer. *Bound.-Layer Meteor.,* **61,** 389–405.

Deardorff, J. W., G. E. Willis, and B. H. Stockton, 1980: Laboratory studies of the entrainment zone of a convectively mixed layer. *J. Fluid Mech.,* **100,** 41–64.

Eberhard, W. L., R. E. Cupp, and K. R. Healy, 1989: Doppler lidar measurement of profiles of turbulence and momentum flux. *J. Atmos. Oceanic Technol.,* **6,** 809–819.

Eichinger, W. E., D. I. Cooper, D. B. Holtkamp, R. R. Karl Jr., C. R. Quick, and J. J. Tiee, 1993: Derivation of water vapor fluxes from lidar measurements. *Bound.-Layer Meteor.,* **63,** 39–64.

Eilts, M. D., A. Sundara-Rajan, and R. J. Evans, 1987: Estimation of the average surface heat flux over an inhomogeneous terrain from the vertical velocity variance. *Bound.-Layer Meteor.,* **39,** 87–91.

Eloranta, E. W., and D. K. Forrest, 1986: Generation of attenuation corrected lidar images from lidar data. *13th Int. Lidar Conf.,* Toronto, ON, Canada, NASA, 291–294.

Frisch, A. S., B. E. Martner, and J. S. Gibson, 1989: Measurement of the vertical flux of turbulent kinetic energy with a single Doppler radar. *Bound.-Layer Meteor.,* **49,** 331–337.

Gal-Chen, T., M. Xu, and W. L. Eberhard, 1992: Estimations of atmospheric boundary layer fluxes and other turbulence parameters from Doppler lidar data. *J. Geophys. Res.,* **97,** 18 409–18 423.

Grund, C. J., 1996: High resolution Doppler lidar employing a diode pumped injection-seeded Tm:Lu, YAG transmitter. *Advanced Solid-State Lasers,* S. Payne and C. Pollack, Eds., Optical Society of America, 204–206.

——, 1997: High resolution Doppler lidar measurements of wind and turbulence. *Advances in Atmospheric Remote Sensing with Lidar,* A. Ansman, R. Neuber, T. Rairoux, and U. Wandinger, Eds., Springer-Verlag, 235–238.

——, and E. W. Eloranta, 1991: University of Wisconsin high spectral resolution lidar. *Opt. Eng.,* **30,** 6–12.

Horst, T. W., and J. C. Weil, 1994: How far is far enough? The fetch requirements for micrometeorological measurement of surface fluxes. *J. Atmos. Oceanic Technol.,* **11,** 1018–1025.

Kaimal, J. C., J. C. Wyngaard, D. A. Haugen, O. R. Cote, Y. Isumi, S. J. Caughey, and C. J. Readings, 1976: Turbulence structure in the convective boundary layer. *J. Atmos. Sci.,* **33,** 2152–2169.

Kiehl, J. T., 1992: Atmospheric general circulation modeling. *Climate System Modeling,* K. E. Trenberth, Ed., Cambridge University Press, 319–369.

Kiemle, C., G. Ehret, A. Giez, K. J. Davis, D. H. Lenschow, and S. P. Oncley, 1998: Estimation of boundary-layer humidity fluxes and statistics from airborne Differential Absorption Lidar (DIAL). *J. Geophys. Res.,* **102** (D24), 29 189–29 203.

Kovalev, V. A., 1993: Lidar measurement of the vertical aerosol extinction profiles with range dependent backscatter-to-extinction ratios. *Appl. Opt.,* **32,** 6053–6065.

Lauritsen, D., Z. Malekmadani, C. Morel, and R. McBeth, 1987: The Cross-chain Loran Atmospheric Sounding System (CLASS). Preprints, *Sixth Symp. on Meteor. Observations and Instrumentation,* New Orleans, LA, Amer. Meteor. Soc., 340–343.

LeMone, M. A., 1990: Some observations of vertical velocity skewness in the convective planetary boundary layer. *J. Atmos. Sci.,* **47,** 1163–1169.

Lenschow, D. H., 1970: Airplane measurements of planetary boundary layer structure. *J. Appl. Meteor.*, **9,** 874–884.

——, J. Mann, and L. Kristensen, 1994. How long is long enough when measuring fluxes and other turbulence statistics? *J. Atmos. Oceanic Technol.*, **11,** 661–673.

Lewis, J. M., 1997: The Lettau–Schwerdtfeger balloon experiment: Measurement of turbulence via Austuasch theory. *Bull. Amer. Meteor. Soc.*, **78,** 2619–2635.

Liou, Y.-C. and D. K. Lilly, 1997: Numerical study of the structure and evolution of a heated planetary boundary layer with a jet. *J. Geophys. Res.*, **102,** 4447–4462.

Mahrt, L., and N. Gamage, 1987: Observations of turbulence in stratified flow. *J. Atmos. Sci.*, **44,** 1106–1121.

Mann, J., K. J. Davis, D. H. Lenschow, S. P. Oncley, C. Kiemle, G. Ehret, A. Giez, and H. G. Schreiber, 1995: Airborne observations of the boundary layer top, and associated gravity waves and boundary layer structure. Preprints, *Ninth Symp. on Meteorological Observations and Instrumentation,* Charlotte, NC, Amer. Meteor. Soc., 113–116.

Mayor, S. D., 1995: Evaluation of the NCAR Doppler lidar and applications to measuring boundary layer structure. NCAR Cooperative Thesis 156, 88 pp. [Available from NCAR, P. O. Box 3000, Boulder, CO 80307-3000.]

——, D. H. Lenschow, R. L. Schwiesow, J. Mann, C. L. Frush, and M. K. Simon, 1997: Validation of NCAR 10.6-μ CO_2 Doppler lidar radial velocity measurements and comparison with a 915-MHz profiler. *J. Atmos. Oceanic Technol.*, **14,** 1110–1126.

Measures, R. M., 1984: *Laser Remote Sensing: Fundamentals and Applications.* Wiley, 510 pp.

Militzer, J. M., M. C. Michalis, S. R. Semmer, K. S. Norris, T. W. Horst, S. P. Oncley, A. C. Delany, and F. V. Brock, 1995: Development of the prototype PAM III/Flux-PAM surface meteorological station. Preprints, *Ninth Symp. on Meteorological Observations and Instrumentation,* Charlotte, NC, Amer. Meteor. Soc., 490–494.

Moeng, C.-H., and R. Rotunno, 1990: Vertical-velocity skewness in the buoyancy-driven boundary layer. *J. Atmos. Sci.*, **47,** 1149–1162.

Nastrom, G. D., and T. E. VanZandt, 1994: Mean vertical motions seen by radar wind profilers. *J. Appl. Meteor.*, **33,** 984–995.

Nieuwstadt, F. T. M., and R. A. Brost, 1986: The decay of turbulence around sunset. *J. Atmos. Sci.*, **43,** 543–546.

Parsons, D., and Coauthors, 1994: The Integrated Sounding System: Description and preliminary observations from TOGA COARE. *Bull. Amer. Meteor. Soc.*, **75,** 553–567.

Post, M. J., and R. E. Cupp, 1990: Optimizing a pulsed Doppler lidar. *Appl. Opt.*, **29,** 4145–4158.

Senff, C., R. J. Alvarez II, S. D. Mayor, and Y. Zhao, 1996: Ozone flux profiles in the boundary layer observed with an ozone DIAL Doppler lidar combination. *Advances in Atmospheric Remote Sensing with Lidar*, A. Ansmann, R. Neuber, P. Rairoux, and U. Wandinger, Eds., Springer-Verlag, 363–366.

Shaw, W. J., and S. Zhong, 1994: On the measurement of momentum flux profiles using a five-beam 915-MHz wind profiler. *Proc. Third Int. Symp. on Tropospheric Profiling: Needs and Technologies,* Hamburg, Germany, Max-Planck-Gesellschaft zur Förderung der Wissenschaften, S475–S477.

Sisterson, D., and P. Frenzen, 1978: Nocturnal boundary-layer wind maxima and the problem of wind power assessment. *Environ. Sci. Technol.*, **12,** 218–221.

Stensrud, D. J., 1996: Importance of low-level jets to climate: A review. *J. Climate,* **9,** 1698–1711.

Stull, R. B., 1988: *An Introduction to Boundary Layer Meteorology.* Kluwer Academic Publishers, 666 pp.

Wakimoto, R. M., 1982: The life cycle of thunderstorm gust fronts as viewed with Doppler radar and rawinsonde data. *Mon. Wea. Rev.*, **110,** 1060–1082.

Weckwerth, T. M., C. J. Grund, and S. D. Mayor, 1997: Linearly organized coherent structures in the surface layer. Preprints, *12th Symp. on Boundary Layers and Turbulence*, Vancouver, BC, Canada, Amer. Meteor. Soc., 22–23.

Whiteman, C. D., X. Bian, and S. Zhong, 1997: Low-level jet climatology from enhanced rawinsonde observations at a site in the southern Great Plains. *J. Appl. Meteor.*, **36,** 1363–1376.

Wilczak, J. M., E. E. Gossard, W. D. Neff, and W. L. Eberhard, 1996: Ground-based remote sensing of the atmospheric boundary layer: 25 years of progress. *Bound.-Layer Meteor.*, **78,** 321–349.

Wurman, J., J. Straka, E. Rasmussen, M. Randall, and A. Zahrai, 1995: Design and first results from a portable, pencil-beam, pulsed Doppler radar. Preprints, *27th Conf. on Radar Meteorology,* Vail, CO, Amer. Meteor. Soc., 713–716.

Young, G. S., 1988: Turbulence structure of the convective boundary layer. Part I: Variability of normalized turbulence statistics. *J. Atmos. Sci.*, **45,** 719–726.

Zhao, Y., J. N. Howell, and R. M. Hardesty, 1994: ETL's Transportable Lower Troposphere Ozone Lidar. Preprints, *17th Int. Laser Radar Conf.* Sendai, Japan, Laser Radar Society of Japan, 248–250.